A Computational Tool for Monte Carlo Simulations of Biomolecular Reaction Networks Modeled on Physical Principles

Isaac T. S. Li, Evan Mills, and Kevin Truong*, *Member, IEEE*

***Abstract*—Deciphering and designing complex biomolecular networks in the cell are the goals of systems and synthetic biology, respectively. The effects of localization, spatial heterogeneity, and molecular fluctuations in biomolecular networks are not well understood. We present a theoretical approach based on physical principles to accurately simulate biomolecular networks using the Monte Carlo method. Incorporating this theory, a computational tool named Monte Carlo biomolecular simulator (MBS) was developed, enabling studies of biomolecular kinetics with both spatial and temporal resolutions. The accuracy of MBS was verified by comparison against the classical deterministic approaches. Furthermore, the effects of localization, spatial heterogeneity, and molecular fluctuations were studied in three simulated model systems, showing their impact on the overall reaction kinetics. This work demonstrates the unique insights that can be discovered by considering the subtle effects that can be created by the spatial and temporal kinetics of biomolecular reaction networks.**

***Index Terms*—Biomolecular reaction networks, Monte Carlo simulation, spatiotemporal resolution.**

I. Introduction

CELLS are complex biological systems made of networks of biomolecular reactions [1]. The study of the kinetic behavior of these networks is crucial to understanding the intricacies of their resulting cellular behaviors. Most biomolecular studies to date have focused on the interactions and reaction mechanisms among a small number of proteins and other biomolecules such as nucleotides, metabolites, and ions [2]–[5]. This pioneering work has provided the foundation to study larger and more sophisticated biomolecular reaction networks in the cell. These networks have distinct characteristics. First, biomolecules in the cell such as proteins, DNA, ions, and metabolites are spatially organized into compartments or anchored to membranes. It is still largely unknown how the localization of these molecules provides signaling, control, and functional advantages to the cell. Second, many biomolecular reactions such as the Ca^{2+} wave and the action potential involve both temporal and spatial kinetics. Thus, a molecular concentration profile in time and space is critical for studying these networks. Lastly, restricted by the size and organization of the cell, the population of certain molecular species such as protein encoding DNA could be as low as single digits. Reactions involving low-copy-number species have large statistical fluctuation in activities, affecting the stability and variability of the reaction network. Therefore, being able to simulate all the aforementioned aspects of biomolecular reactions is crucial for understanding their resulting cellular behaviors.

There are two classes of approaches to simulate biomolecular reactions: deterministic and stochastic. The most common deterministic approach to study biomolecular kinetics is by ordinary differential equations (ODEs), which usually assumes homogeneous concentration for all biomolecular species within the reaction volume. Therefore, ODE would not provide the desired spatial resolution. One could obtain spatial information by applying a system of second-order partial differential equations (PDEs). However, deriving and solving a large system of equations needed for spatial resolution becomes more challenging as the number of interactions increases, often requiring many approximations. Furthermore, the effect of molecular fluctuation for low-copy-number molecular species cannot be easily handled by a deterministic model. To resolve these problems, we created a computational tool named Monte Carlo Biomolecular Reaction Simulator (MBS) that used a stochastic model to simulate the motion and reaction of each molecule in user-defined spaces. While many computational tools have been used to simulate signaling pathways and biomolecular oscillations (for example, StochSim [6], Virtual Cell [7], BioNetS [8], E-Cell [9], SmartCell [10], ChemCell [11], Meredys, STEPS [12], etc. [13]–[23]), many of these tools either lacked the stochastic or spatial considerations of MBS. The computational tools [6], [16] that considered these effects adopted convenient but crude approximations of physical principles for the handling of single-molecule diffusion and reaction probability. Thus, using the same physical approximations, we could not produce simple diffusion and reaction rate constants. Consequently, in our computational tool (MBS), we developed a set of physically realistic models to represent the diffusion and reaction processes. First,

Manuscript received November 21, 2008; revised August 18, 2009. First published November 3, 2009; current version published March 24, 2010. This work was supported by the Canadian Institutes of Health Research under Grant 81262, by the Heart and Stroke Foundation under Grant NA6241, and by the Natural Science and Engineering Research Council under Grant 283170. *Asterisk indicates corresponding author.*

I. T. S. Li was with the Institute of Biomaterials and Biomedical Engineering, University of Toronto, Toronto, ON M5S 3G9, Canada. He is now with the Department of Chemistry, University of Toronto, Toronto, ON M5S 3G9, Canada (e-mail: isaac.li@utoronto.ca).

E. Mills is with the Institute of Biomaterials and Biomedical Engineering, University of Toronto, Toronto, ON M5S 3G9, Canada (e-mail: e.mills@utoronto.ca).

*K. Truong is with the Institute of Biomaterials and Biomedical Engineering and the Edward S. Rogers Sr. Department of Electrical and Computer Engineering, University of Toronto, Toronto, ON M5S 3G9 Canada (e-mail: kevin.truong@utoronto.ca).

Color versions of one or more of the figures in this paper are available online at http://ieeexplore.ieee.org.

Digital Object Identifier 10.1109/TNB.2009.2035114

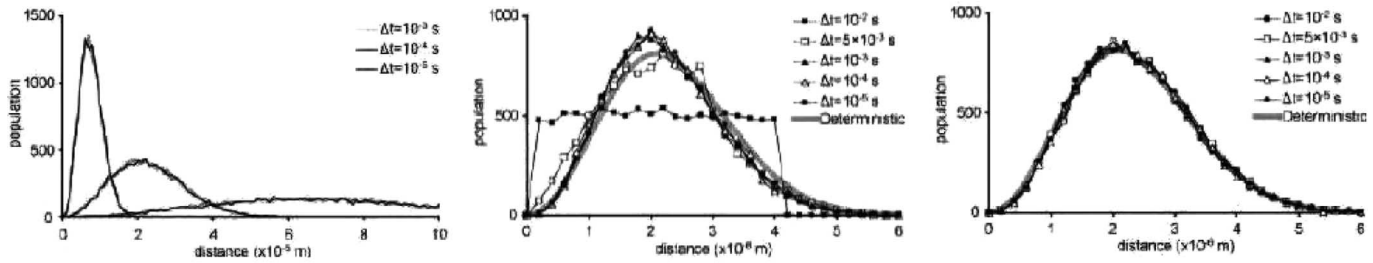

Fig. 1. (a) Population distribution of 10^4 molecules. The molecules were diffused from a single point as a function of their distances from the origin of diffusion. The three distinctive peaks at distances of 10, 20, and 60 μm were the population distribution of different total time durations of 10, 100, and 1000 ms, respectively. The three shades were simulations under different time step duration $\Delta t = 10^{-3}$ s (lighter gray), 10^{-4} s (darker gray), and 10^{-5} s (black). The population distribution of (b) uniform step size distribution model and (c) our diffusion model. Both simulations had a total duration of 0.1 s. The deterministic solution was indicated as the thick gray line. The population distributions using five time step durations $\Delta t = 10^{-2}$ s (solid square), 5×10^{-3} s (hollow square), 10^{-3}s (solid triangle), 10^{-4} s (hollow triangle), and 10^{-5} s (solid circle) were compared with the deterministic solution.

the validity of these models was verified by showing that it could produce diffusion and reaction rate constants. Next, the tool was applied to model complex systems, including a predator–prey system, genetic oscillator, and Ca^{2+} wave.

II. Results and Discussion

A. Diffusion

Our diffusion model accurately described the physical process of diffusion. Since the physical diffusion process is independent of simulation time step durations (Δt), a difference in Δt should ideally not affect the diffusion kinetics. To test this condition, 10^4 molecules were placed at a single point and diffused with various Δt. The population distributions were identical using different Δt in the simulations at three different total simulation durations [see Fig. 1(a)]. Furthermore, these density distributions all coincided with the deterministic distribution described by the macroscopic diffusion equation

$$\frac{\partial \phi(\vec{r}, t)}{\partial t} = D\nabla^2 \phi(\vec{r}, t)$$

where D was the diffusion coefficient, φ was the density distribution, $\vec{r}$ was the vector from the center of diffusion to the point of interest, and t was the total duration of diffusion [see Fig. 1(c)]. Thus, our diffusion model produced the correct spatial profile of molecules, which provided a solid foundation for accurately assessing reaction kinetics.

In contrast, a uniform step size model used in recent literature was not accurate in describing the physical process of diffusion. In this model, the random-walk step size used a uniform distribution from 0 to a maximal value depending on D and Δt. A uniform step size model was compared to our diffusion model by simulating a total duration of 10^{-1} s under different Δt's (10^{-1}, 10^{-2}, 10^{-3}, and 10^{-4} s). For these different Δt, the uniform step size model produced population distribution that does not coincide with each other, or with the deterministic solution [see Fig. 1(b)]. The difference was especially evident if Δt was large compared to the total simulation duration. Since reactions in Monte Carlo simulations are handled by finding reaction probabilities that are highly dependent on distances between reagent molecules, an inaccurate spatial distribution of molecules caused by uniform step size model will yield an inaccurate simulation of reaction kinetics.

B. Handling Reaction Basics

At the different time step durations (Δt), our reaction model accurately simulated simple reaction kinetics as the kinetics curves of the simulation coincided with the deterministic curves. For the association reaction defined by

$$A + B \xrightarrow{k_a} C$$

an initial concentration of 198 μM (or 500 molecules per cell) for both A and B was created in a spherical cell with a radius of 1 μm. The association rate constants k_a in the physiological range of 10^3–10^8 $\mathrm{M}^{-1}\cdot\mathrm{s}^{-1}$ were tested. Deterministically, the kinetics of this reaction was described by the differential equation

$$\frac{d[C]}{dt} = k_a[A][B].$$

Since A and B had the same initial concentration A_0, the equation was simplified as

$$\frac{d[C]}{dt} = k_a\left(A_0 - [C]\right)^2.$$

The deterministic curves coincided with the kinetic curves from the simulation in the k_a range of 10^3–10^6 $\mathrm{M}^{-1}\cdot\mathrm{s}^{-1}$ [see Fig. 2(a)]. Furthermore, within this range, the simulation curves with different Δt coincided with the deterministic curves (data not shown). Note that at k_a above 10^7 $\mathrm{M}^{-1}\cdot\mathrm{s}^{-1}$, the deterministic rate of reaction became faster than the simulated rate, as the reaction became diffusion limited. This physical phenomenon occurred in extreme situations when reactions happened faster than molecules could diffuse into areas depleted of reagent molecules. This lowered the effective local concentration of the reagents, and therefore, the speed of reaction became slower. This phenomenon of diffusion-limited reactions was easily captured by our model; however, using a deterministic model, it cannot be captured without additional modifications.

For the dissociation reaction defined by

$$A \xrightarrow{k_d} B + C + \cdots$$

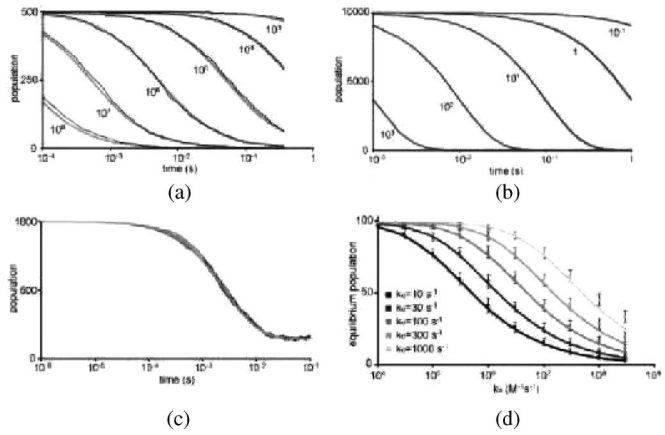

Fig. 2. (a) Population of reagent molecule as a function of time plotted in log scale for association reactions with various rate constant k_a ranging from 10^3 to 10^8 M^{-1} s^{-1}. The Δt was 10^{-4} s and the total duration was 0.5 s. (b) Population of reagent molecule as a function of time plotted in log scale for dissociation reaction with various rate constant k_d ranging from 10^{-1} to 10^3 s^{-1}. The Δt was 10^{-4} s and the total duration was 0.5 s. (c) Reversible reaction kinetics showing population of reagent molecule as a function of time plotted in log scale for association reactions with various simulation time step durations $\Delta t = 10^{-6}$ to 10^{-3} s. In all the aforementioned figures, the simulated kinetics curve (thin black) was compared to the deterministic kinetics curve (thick gray). (d) Simulated equilibrium constants with k_a ranging from 10^4 to 3×10^8 M^{-1} s^{-1} and k_d ranging from 10 to 1000 s^{-1}. Each solid square represented the average simulated equilibrium constants for a particular value of k_a and k_d. The error bar was derived from the fluctuation of molecule population at equilibrium using 1000 equilibrium point. The solid line represented the deterministic solution of the equilibrium point with a given k_d as a function of k_a.

the deterministic rate equation was

$$\frac{d[A]}{dt} = -k_d[A]$$

with solution

$$[A] = [A_0]e^{-k_d t}.$$

Our simulation kinetic curve coincided with the deterministic curves for the entire range of k_d [see Fig. 2(b)]. Again, this agreement was independent of Δt of the simulation (data not shown).

Reversible reactions were studied by combining the association reaction and the dissociation reaction as

$$A + B \underset{k_d}{\overset{k_a}{\rightleftharpoons}} C.$$

At different Δt, the simulated kinetics curves coincided with the deterministic curves and reached the same equilibrium points [see Fig. 2(c)]. To verify this for a broader range of k_a and k_d, 50 reactions with an array of k_a and k_d values were simulated to equilibrium point. For k_a below 10^8 $\mathrm{M}^{-1}\cdot\mathrm{s}^{-1}$, the simulated equilibrium concentration of molecule *C* agreed well with what was expected from deterministic solution. In contrast for k_a above 10^8 $\mathrm{M}^{-1}\cdot\mathrm{s}^{-1}$, as expected, it did not agree since the deterministic solution cannot model diffusion-limited reactions [see Fig. 2(d)].

C. Predator–Prey System

Spatial heterogeneity of a molecular specie arising from molecular fluctuations created local areas of reaction kinetics that differ from the population. The predator–prey system was used to construct a simple spatial and temporal biomolecular oscillator. In this model, there was a constant source of molecule *A* that can be converted into molecule *X* (prey molecule) by molecule *X* at the rate of k_{a1}. Similarly, molecule *X* can be converted into molecule *Y* (predator molecule) by molecule *Y* at the rate of k_{a2}. Lastly, molecule *Y* decayed into molecule *D* at the rate of k_d. The biomolecular network is described as

$$A + X \xrightarrow{k_{a1}} 2X$$
$$X + Y \xrightarrow{k_{a2}} 2Y$$
$$Y \xrightarrow{k_d} D.$$

Deterministically, this was described as follows:

$$\frac{dX(t)}{dt} = k_{a1}A(t)X(t) - k_{a2}X(t)Y(t)$$
$$\frac{dY(t)}{dt} = k_{a2}X(t)Y(t) - k_dY(t)$$

where *A*(*t*), *X*(*t*), and *Y*(*t*) were the concentration over time of *A*, *X*, and *Y*, respectively. The solution to this system of differential equations was a stable oscillation in the concentration of *A*, *X*, and *Y* with a fixed amplitude [see Fig. 3(a) and (b)]. However, our simulation showed that the concentration oscillation varied in amplitude peak and phase [see Fig. 3(c) and (d)]. While the reaction started with a spatial homogeneity of molecular species, as reactions occurred, it created local areas of spatial heterogeneity [see Fig. 3(e)]. The differences in local concentrations caused local differences in the reaction kinetics, resulting in off-phase concentration oscillations. Since the overall oscillation was a superposition of the local oscillations, off-phased local oscillations caused an overall oscillation that was less coherent and had varying amplitude peaks.

The effect of spatial heterogeneity was reduced by a larger diffusion coefficient (such as 10^{-10} m^2/s), which made the molecular species more homogenous over the course of the simulation. Using this diffusion coefficient, the peak amplitude of population oscillation was less varied, resembling the oscillatory amplitude of the deterministic solution [see Fig. 3(f)]. In addition, because the amplitude was smaller, the oscillation frequency was higher, as it took less time to traverse the predator–prey population phase space where the path length was shorter. In contrast, a small diffusion coefficient (10^{-12} m^2/s) made the molecules less mobile, and hence, kept the molecular species more localized. Therefore, a large local concentration can be achieved, which lowered the oscillation frequency (data not shown). Hence, the diffusion coefficient played an important role in determining biomolecular kinetics.

D. Prokaryotic and Eukaryotic Genetic Oscillator

The spatial localization of molecules into cellular compartments changed the amplitude or phase of the genetic oscillator.

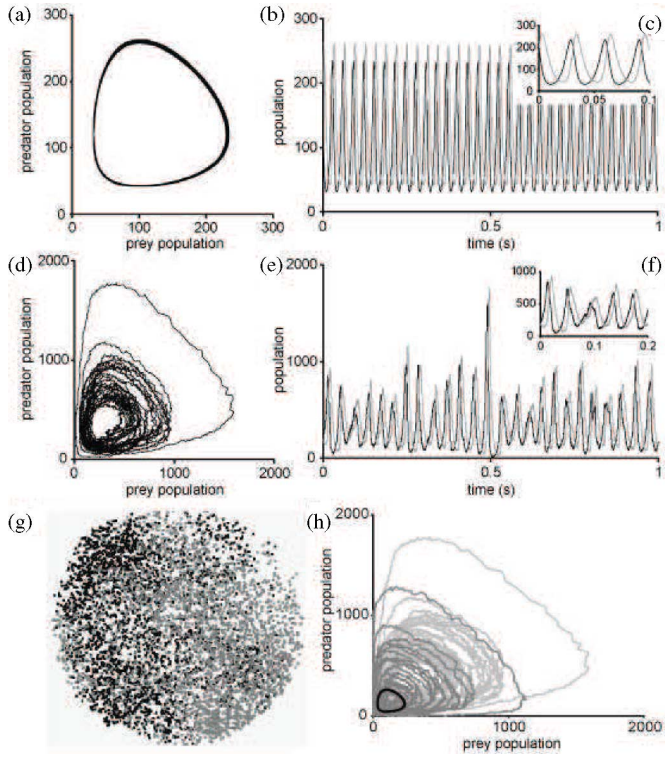

Fig. 3. Deterministic solutions of (a) phase space predator (molecule *Y*) population versus prey (molecule *X*) population, (b) predator (gray) and prey (black) population over time, (c) zoomed graph of (b). Monte Carlo simulation solution of (d) phase space predator population versus prey population, (e) predator (gray) and prey (black) population over time, (f) zoomed graph of (e). (g) Reaction mixture with spatial heterogeneity of prey (black dots) and predator (gray dots) molecules. (h) Phase space predator (molecule *Y*) population versus prey (molecule *X*) population of simulations with different diffusion coefficients. Lower diffusion coefficient (lighter gray) resulted in curves with greater amplitudes while higher diffusion coefficient (darker gray) shifted the curves toward the bottom left corner. The deterministic solution was shown in black.

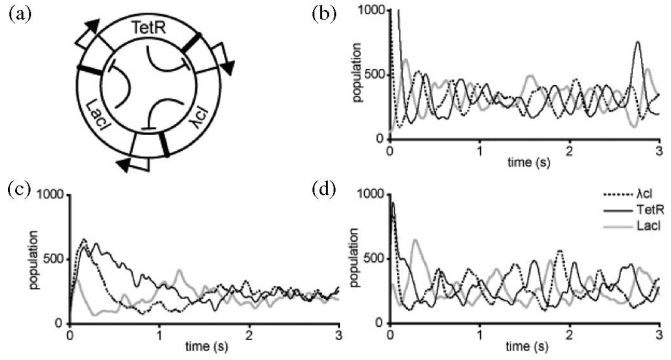

Fig. 4. (a) Plasmid schematic of a genetic oscillator. Regions with arrows were repressor binding regions of the plasmid DNA. Regions marked with λcI, TetR, and LacI are the genes regulated by their respective repressor binding regions. (b) Population changes of the three repressor proteins in the prokaryotic model. Population oscillations of the three repressor proteins in the eukaryotic model with (c) low nuclear membrane transport rates of $5 \times 10^3\ \mathrm{s}^{-1}$ and (d) high nuclear membrane transport rate of $5 \times 10^5 \mathrm{s}^{-1}$. Dotted lines represented λcI; solid black, TetR; solid grey, LacI.

To study the effect of molecular localization into compartments, a prokaryotic genetic oscillator was compared to a eukaryotic genetic oscillator. In our prokaryotic oscillator, mRNA was transcribed and translated into proteins in the cytoplasm. These translated protein then regulated gene expression by interacting with genetic material in the cytoplasm. Conversely, in our eukaryotic oscillator, mRNA was transcribed inside the nucleus, and then transported outside the nucleus where mRNA was translated into proteins. For these translated protein to regulate gene expression, they were transported back into the nucleus. Since transcription and translation were relatively slow reactions, low reaction rate constants were used. Thus, any biomolecular species had sufficient time to reach spatial homogeneity within its own compartment before the reaction kinetics changed significantly.

The genetic network was constructed to produce oscillating concentrations of three different species of proteins each with a phase shift, as previously described [17] [see Fig. 4(a)]. The network was composed of three repressor proteins (tetR, lacI, and λcI) forming a cyclic negative feedback loop—each inhibiting the expression of one other repressor [see Fig. 4(a)]. The repressor protein and mRNAs were constantly degraded by intracellular proteases and RNase. For instance, if the expression of tetR was inhibited, tetR protein concentration decreased. This decrease released the repression of λcI, causing the concentration of λcI to increase. This cycle propagated and repeated to create an oscillation in the concentration of each of the repressor proteins with the same delay from each other. Transcription, translation, and degradation (of both protein and mRNA) were modeled in our simulation as simple first-order reactions. For comparison purposes, the synthesis and degradation rates of mRNA and protein were the same for both prokaryotic and eukaryotic cells. The binding between the regulatory regions of the plasmid DNA and the three repressor proteins were modeled as reversible reactions with the same dissociation constants in both systems.

In the simulation of the prokaryotic case, the three repressor proteins oscillated with $2\pi/3$ phase difference, as expected due to the symmetry of the system [see Fig. 4(b)], while the oscillation characteristics of the eukaryotic was dependent on the transport of biomolecules across the nuclear membrane. As expected in the prokaryotic oscillator, the molecular fluctuation caused the variations in both the amplitude and phase of the oscillations similar to the predator–prey system. In the eukaryotic oscillator, the periodic oscillation pattern was no longer observed in the simulation when using the same set of initial conditions [see Fig. 4(c)]. This was due to insufficient transport of mRNA and proteins across the nuclear membrane. The statistical fluctuation of the nuclear import and export rate in combination with the phase delay caused by the nuclear transport disrupted the synchrony between the protein expression and gene repression. This caused the concentration oscillation of the three repressor proteins to be off from the $2\pi/3$ phase, and hence, the chaotic fluctuation [see Fig. 4(c)]. When the rate of nuclear transport was sufficiently high, the oscillation returned because the phase delay became negligible between the cytoplasmic and the nuclear concentration [see Fig. 4(d)]. Thus, the

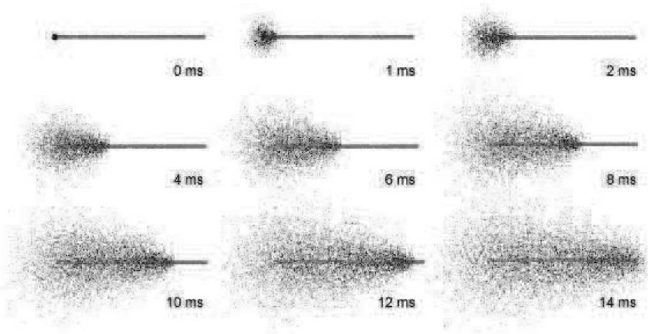

Fig. 5. Spatial propagation of the Ca^{2+} over 14 ms. Top-left corner showed the triggering Ca^{2+} event at $t = 0$ ms. The Ca^{2+} propagation (horizontal extension to the right) distributed faster than diffusion (vertical).

creation of a genetic oscillator in a eukaryotic cell will be more challenging than the prokaryotic case.

E. Ca^{2+} Wave

Our simulations showed that the kinetics of Ca^{2+} wave propagation depended on the density and geometric arrangement of the Ca^{2+} channels. Through the highly regulated events of intracellular Ca^{2+} homeostasis, often seen as a Ca^{2+} concentration wave, Ca^{2+} regulates numerous physiological cellular phenomena, including development, differentiation, and apoptosis. When triggered by other secondary messengers such as inositol-1,4,5-triphosphate (IP_3), Ca^{2+} is released from the endoplasmic reticulum (ER) to the cytoplasm by channels such as the IP_3 receptor [24], [25]. To simulate a Ca^{2+} concentration wave, we modeled the Ca^{2+}-induced-Ca^{2+}-release mechanism, where the membrane Ca^{2+} channels were opened when they bound to Ca^{2+} from the outside. A cylindrical compartment representing the ER was lined with Ca^{2+} channels and filled with Ca^{2+}. Hence, when a dose of Ca^{2+} was added outside at one end of the cylindrical compartment, the closest Ca^{2+} channel bound Ca^{2+} and released Ca^{2+} from inside. Subsequently, this recently released Ca^{2+} diffused into the surrounding space. Since the local area outside the recently opened Ca^{2+} channels had the highest concentration of Ca^{2+}, the edge of the Ca^{2+} diffusion triggered the adjacent channel to release Ca^{2+}. Thus, a region with the highest Ca^{2+} concentration propagates along the membrane of the cylindrical compartment like a wave (see Fig. 5).

The surface density of Ca^{2+} channels, as well as their Ca^{2+} transport rate, affected the speed of wave propagation. In these simulations, the Ca^{2+} channel release rate was in the same order as Ca^{2+} diffusion. If the binding and channel-opening events were slower than Ca^{2+} diffusion, the speed of Ca^{2+} wave was dominated by diffusion, resulting in a wave propagation less guided by the cylinder [see Fig. 6(c)]. Conversely, if the binding and channeling opening were faster than Ca^{2+} diffusion, the wave propagation speed was faster than diffusion [see Fig. 6(c)]. The Ca^{2+} channel density also played a very vital role to the propagation of the Ca^{2+}. In the case with 1000 channels on the membrane, there were sufficient channels on the membrane to maintain a high Ca^{2+} release rate of $\sim$420 ions/ms until 14 ms

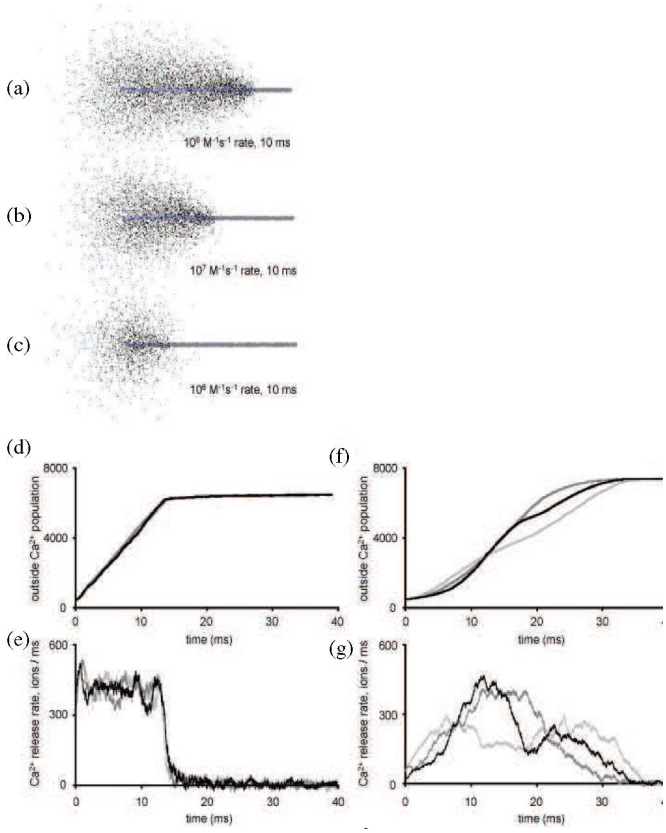

Fig. 6. Graphical representation of the Ca^{2+} distribution after 10 ms for experiments with different channel binding/opening rate. (a) 10^8 M^{-1} s^{-1}. (b) 10^7 M^{-1} s^{-1}. (c) 10^6 M^{-1} s^{-1}. (d) Ca^{2+} population outside the compartment over time for 1000 membrane channels. (e) Ca^{2+} release rate over time for 1000 membrane channels. (f) Ca^{2+} population outside the compartment over time for 100 membrane channels. (g) Ca^{2+} release rate over time for 100 membrane channels. Black, dark gray, and light gray lines in each figure [(d)–(g)] are three simulations using the same setup parameters.

[see Fig. 6(d) and (e)]. At 14 ms, the Ca^{2+} release rate decreased to 0 as the propagation reached the end of the cylindrical compartment. Multiple runs of the same simulation showed that the propagation rate and the duration of propagations are consistent [see Fig. 6(d) and (e)]. In contrast, in the case with only 100 channels on the membrane, the propagation along the cylindrical chamber required Ca^{2+} release rate over twice as long as in the case of 1000 membrane channels for an average of 32 ms [see Fig. 6(f)].

Additionally, the Ca^{2+} release rate was no longer uniform throughout the propagation [see Fig. 6(g)] and even the pattern of release rate was different among simulations with the same setup parameters [see Fig. 6(f) and (g)]. This is due to decreased uniformity of membrane channels along the axial direction as the number of membrane channels is lowered. In a situation with nonuniform distribution of membrane channels, the regions with higher channel density has a faster propagation rate and *vice versa*. For instance, the simulation shown as black curves in Fig. 6(f) and (g) had a faster Ca^{2+} release, and consequently, faster propagation rate until 15 ms after the propagation started. The propagation then slowed down due to sparser channels in the middle section of the cylinder.

F. Applicability to Other Biological Problems

Here, we presented a program for spatial/stochastic modeling based on the accurate description of the physics on single-molecule reactions. This study can be modified easily to account for various interesting and challenging problems, specific to biology. For instance, by adding intermediate reversible reactions of a reactive species, we can create different intermediate states of the species, each having their unique physical and chemical properties. The diffusion behavior of the molecules can be modified by changing the step size distribution function that allows us to create diffusion behavior from subdiffusion to superdiffusion. We could also create compartments that are semipermeable by creating pores with different permeability inside the membrane. We model the pores as a reactive species with the molecules that are allowed to go through the membrane. The association and dissociation kinetics determine the permeability of molecules across the membrane. In general, the program is designed such that all phenomenological rate constants can be converted to a representative reaction rate constant, allowing the use of simple models that describe reactions alone to capture the physics of many other phenomena.

G. Design Considerations of Spatial/Stochastic Software

Besides the apparent difference and advantage between our program, and the programs that use PDEs, our program has the simplicity that every rate-limited phenomena can be modeled by a reaction. This allowed the use of rate constants determined elsewhere directly in our simulation by converting it to a reaction rate constant. Similar to some other Monte Carlo programs that consider the diffusion and reaction of each particle, our model considered them as well. Our physical model was derived and tested from first principle that faithfully reproduced the observed reaction rate constants. Due to the lack of details about the physical models used in other Monte Carlo programs, we cannot offer a direct comparison of the physical models used in our program.

At the moment, the program cannot run in a parallel fashion, but it is possible with some modifications of the source code to take advantage of the multiple processors that commonly exists in modern CPUs and general-purpose utilities (GPUs). In particular, parallel processing is possible within each reaction time step. Since the computer is constantly computing the probability of reaction of each molecule within each time step and these events are independent of each other, this computation can be performed in parallel. In contrast, parallel processing between steps of the simulation is not feasible because the current spatial locations of the molecules influence the reaction and location of molecules in the following time steps.

III. Methods and Supplemental Information

A. Methods

Detailed methods are available online
http://apel.ibbme.utoronto.ca/apel/software/mbs_methods.pdf

B. Example: Engineering a Molecular D-Latch

A detailed example is available online
http://apel.ibbme.utoronto.ca/apel/software/mbs_latch.pdf

C. Software

This software is available online
http://apel.ibbme.utoronto.ca/apel/software
Name: Monte Carlo Biomolecular Reaction Simulator
Programming language: C/C++
License: Open-source and free for academic and nonprofit use only

IV. Conclusion

In this paper, we described the creation of a computational tool using a Monte Carlo approach for simulating the spatial and temporal kinetics of biomolecular reaction networks within a cell. Since our models were based on physical principles, the tool accurately produced diffusion and reaction constants across a range of time step durations. Simulations on a predator–prey system demonstrated the phenomenon of spatial heterogeneity and its effect on the frequency and amplitude of the oscillation. Subsequent simulations on prokaryotic and eukaryotic genetic oscillators demonstrated transport of proteins and mRNA across a nuclear compartment disturbs the oscillation. In fast reactions such as Ca^{2+} waves, density and geometric arrangement of the Ca^{2+} channels affect the speed of Ca^{2+} wave propagation. Together, this paper demonstrates the unique insights that can be discovered by considering the subtle effects that can be created by the spatial and temporal kinetics of biomolecular reaction networks. Future applications of the computational tool include designing synthetic networks or modeling larger existing biological networks.

References

[1] G. Weng, U. S. Bhalla, and R. Iyengar, "Complexity in biological signaling systems," *Science*, vol. 284, pp. 92–96, 1999.
[2] M. T. Borisuk and J. J. Tyson, "Bifurcation analysis of a model of mitotic control in frog eggs," *J. Theor. Biol.*, vol. 195, pp. 69–85, 1998.
[3] K. C. Chen, A. Csikasz-Nagy, B. Gyorffy, J. Val, B. Novak, and J. J. Tyson, "Kinetic analysis of a molecular model of the budding yeast cell cycle," *Mol. Biol. Cell.*, vol. 11, pp. 369–391, 2000.
[4] J. S. Edwards, R. U. Ibarra, and B. O. Palsson, "In silico predictions of Escherichia coli metabolic capabilities are consistent with experimental data," *Nat. Biotechnol.*, vol. 19, pp. 125–130, 2001.
[5] M. Morohashi, A. E. Winn, M. T. Borisuk, H. Bolouri, J. Doyle, and H. Kitano, "Robustness as a measure of plausibility in models of biochemical networks," *J. Theor. Biol.*, vol. 216, pp. 19–30, 2002.
[6] N. L. Novere and T. S. Shimizu, "STOCHSIM: Modelling of stochastic biomolecular processes," *Bioinformatics*, vol. 17, pp. 575–576, 2001.
[7] I. I. Moraru, J. C. Schaff, B. M. Slepchenko, and L. M. Loew, "The virtual cell: An integrated modeling environment for experimental and computational cell biology," *Ann. N.Y. Acad. Sci.*, vol. 971, pp. 595–596, 2002.
[8] D. Adalsteinsson, D. McMillen, and T. C. Elston, "Biochemical network stochastic simulator (BioNetS): Software for stochastic modeling of biochemical networks," *BMC Bioinf.*, vol. 5, no. 24, 2004.
[9] M. Tomita, K. Hashimoto, K. Takahashi, T. S. Shimizu, Y. Matsuzaki, F. Miyoshi, K. Saito, S. Tanida, K. Yugi, J. C. Venter, and C. A. Hutchison, "E-CELL: Software environment for whole-cell simulation," *Bioinformatics*, vol. 15, pp. 72–84, 1999.
[10] M. Ander, P. Beltrao, B. D. Ventura, J. Ferkinghoff-Borg, M. Foglierini, A. Kaplan, C. Lemerle, I. Tomas-Oliveira, and L. Serrano, "SmartCell,

a framework to simulate cellular processes that combines stochastic approximation with diffusion and localisation: Analysis of simple networks," *Syst. Biol. (Stevenage)*, vol. 1, pp. 129–138, 2004.
[11] A. Slepoy and S. J. Plimpton, "Microbial cell modeling via reacting diffusing particles," *J. Phys.*, vol. 16, pp. 305–309, 2005.
[12] E. D. Schutter and S. Wils, "STEPS: Modeling and simulating complex reaction–diffusion systems with Python," *Frontiers Neuroinf.*, vol. 3, pp. 1–8, 2009.
[13] A. Arkin, J. Ross, and H. H. McAdams, "Stochastic kinetic analysis of developmental pathway bifurcation in phage lambda-infected Escherichia coli cells," *Genetics*, vol. 149, pp. 1633–1648, 1998.
[14] L. Mao and H. Resat, "Probabilistic representation of gene regulatory networks," *Bioinformatics*, vol. 20, pp. 2258–2269, 2004.
[15] T. C. Meng, S. Somani, and P. Dhar, "Modeling and simulation of biological systems with stochasticity," *In Silico Biol.*, vol. 4, pp. 293–309, 2004.
[16] C. Sanford, M. L. Yip, C. White, and J. Parkinson, "Cell++−−simulating biochemical pathways," *Bioinformatics*, vol. 22, pp. 2918–2925, 2006.
[17] M. B. Elowitz and S. Leibler, "A synthetic oscillatory network of transcriptional regulators," *Nature*, vol. 403, pp. 335–338, 2000.
[18] M. B. Elowitz, A. J. Levine, E. D. Siggia, and P. S. Swain, "Stochastic gene expression in a single cell," *Science*, vol. 297, pp. 1183–1186, 2002.
[19] P. S. Swain, M. B. Elowitz, and E. D. Siggia, "Intrinsic and extrinsic contributions to stochasticity in gene expression," *Proc. Nat. Acad. Sci. USA*, vol. 99, pp. 12795–12800, 2002.
[20] S. S. Andrews and D. Bray, "Stochastic simulation of chemical reactions with spatial resolution and single molecule detail," *Phys. Biol.*, vol. 1, pp. 137–151, 2004.
[21] J. Hattne, D. Fange, and J. Elf, "Stochastic reaction–diffusion simulation with MesoRD," *Bioinformatics.*, vol. 21, pp. 2923–2924, 2005.
[22] G. E. Sosinsky, T. J. Deerinck, R. Greco, C. H. Buitenhuys, T. M. Bartol, and M. H. Ellisman, "Development of a model for microphysiological simulations: Small nodes of Ranvier from peripheral nerves of mice reconstructed by electron tomography," *Neuroinformatics*, vol. 3, pp. 133–162, 2005.
[23] T. T. Marquez-Lago and K. Burrage, "Binomial tau-leap spatial stochastic simulation algorithm for applications in chemical kinetics," *J. Chem. Phys.*, vol. 127, pp. 104101–104109, 2007.
[24] I. Bezprozvanny, "Inositol (1,4,5)-trisphosphate receptors: Functional properties, modulation, and role in calcium wave propagation," *Soc. Gen. Physiol. Ser.*, vol. 51, pp. 75–86, 1996.
[25] S. V. Straub, D. R. Giovannucci, and D. I. Yule, "Calcium wave propagation in pancreatic acinar cells: Functional interaction of inositol 1,4,5-trisphosphate receptors, ryanodine receptors, and mitochondria," *J. Gen. Physiol.*, vol. 116, pp. 547–560, 2000.
[26] M. Sudol, C. C. Recinos, J. Abraczinskas, J. Humbert, and A. Farooq, "WW or WoW: The WW domains in a union of bliss," *IUBMB Life*, vol. 57, pp. 773–778, 2005.
[27] I. L. Medintz and J. R. Deschamps, "Maltose-binding protein: A versatile platform for prototyping biosensing," *Curr. Opin. Biotechnol.*, vol. 17, pp. 17–27, 2006.
[28] D. Chin and A. R. Means, "Calmodulin: A prototypical calcium sensor," *Trends Cell Biol.*, vol. 10, pp. 322–328, 2000.
[29] Y. Dudai, "Some properties of adenylate cyclase which might be important for memory formation," *FEBS Lett.*, vol. 191, pp. 165–170, 1985.
[30] Y. S. Cho-Chung, "Modulation of adenylate cyclase signalling," *Semin. Cancer Biol.*, vol. 3, pp. 361–367, 1992.
[31] T. L. Poulos, "Soluble guanylate cyclase," *Curr. Opin. Struct. Biol.*, vol. 16, pp. 736–743, 2006.
[32] S. S. Taylor, C. Kim, D. Vigil, N. M. Haste, J. Yang, J. Wu, and G. S. Anand, "Dynamics of signaling by PKA," *Biochim. Biophys. Acta*, vol. 1754, pp. 25–37, 2005.
[33] S. S. Taylor, J. Yang, J. Wu, N. M. Haste, E. Radzio-Andzelm, and G. Anand, "PKA: A portrait of protein kinase dynamics," *Biochim. Biophys. Acta*, vol. 1697, pp. 259–269, 2004.
[34] S. H. Francis and J. D. Corbin, "Cyclic nucleotide-dependent protein kinases: Intracellular receptors for cAMP and cGMP action," *Crit. Rev. Clin. Lab. Sci.*, vol. 36, pp. 275–328, 1999.
[35] F. van den Akker, "Structural insights into the ligand binding domains of membrane bound guanylyl cyclases and natriuretic peptide receptors," *J. Mol. Biol.*, vol. 311, pp. 923–937, 2001.

Isaac T. S. Li received the B.A.Sc. degree in engineering science and the M.A.Sc. degree in biomedical engineering in 2005 and 2007, respectively, from the University of Toronto, Toronto, ON, Canada, where he is currently working toward the Ph.D. degree in physical chemistry.

Evan Mills received the B.A.Sc. degree in engineering science in 2008 from the University of Toronto, Toronto, ON, Canada, where he is currently working toward the M.A.Sc. degree in biomedical engineering.

Kevin Truong (M'05) received the B.A.Sc. degree in computer engineering and the Ph.D. degree in medical biophysics from the University of Toronto, Toronto, ON, Canada, in 1999 and 2003, respectively.

He is currently an Assistant Professor with the University of Toronto.